OPTIMAL DISTRIBUTION OF THE RELAXATION BEHAVIOR OF LINEAR VISCOELASTIC MATERIALS BY THE PARTICLE SWARM OPTIMIZATION METHOD APPLIED TO THE PROBLEM OF A TWISTING SHAFT

BY

YUTA SAITO

THESIS

Submitted in partial fulfillment of the requirements
for the degree of Master of Science in Aerospace Engineering
in the Graduate College of the
University of Illinois at Urbana-Champaign, 2018

Urbana, Illinois

Adviser:

Professor Harry H. Hilton

ABSTRACT

With rise of new manufacturing techniques such as additive manufacturing, there has been an increase in attention in designing components with distributed material properties. Utilizing the benefits of compliant mechanics, a strategic distribution of the relaxation behavior of linear viscoelastic materials was proposed.

The motivation of this research is to outline a mathematical/computational framework for the material distribution optimization problem of a linear viscoelastic material. The distribution of the *relaxation behavior* (coefficients of the Prony series expansion) across the system was obtained to achieve a target performance of the dynamic system by the particle swarm optimization (PSO) method. The (PSO) method was applied to a simple fixed shaft to demonstrate the improvement in the structural response of the system and convergence capability of the method.

While the simulations showed great improvements in the structural response, the lack of thorough search of the solution space to keep the computation time within a reasonable timeframe meant that the method was unable to determine confidently the reaching of a global minimum. Additionally, the time for convergence increased with the increase of the number of nodes that were optimized.

In order to confidently reach the global minimum within a reasonable timeframe, the computational efficiency of the PSO method must be improved such that the particles can thoroughly search the entire solution space. Additionally, the inclusion of additional constraints to ensure the continuity of the moduli across neighboring nodes must be done for the actual construction of the design.

ACKNOWLEDGEMENTS

I would first like to thank my thesis advisor Professor Emeritus Harry H. Hilton of the Aerospace Engineering Department at the University of Illinois at Urbana-Champaign. The door to Prof. Hilton's office was always open whenever I ran into a trouble spot or had questions about my research. He consistently allowed this paper to be my own work but steered me in the right the direction whenever he thought I needed it.

I also gratefully acknowledge the funding received toward my Master of Science degree from the Japan Student Services Organization (JASSO).

TABLE OF CONTENTS

CHAPTER 1
INTRODUCTION

Compliant mechanics transfers motion, force, or energy by the deflection of flexible members rather than from movable joints. They have been applied in the aerospace industry due to its advantage of light weight, built-in damping mechanism, and reduction of the number of components. These characteristics have made it possible to advance new design concepts to enhance flight performance such as morphing wings and in-flight energy harvesting [1].

With the development of modern additive manufacturing techniques, including 3D printing, there has been an increase in attention to producing solid parts with strategically distributed material properties utilizing the advantages of these compliant mechanics. This has stimulated research to explore techniques to design systems incorporating the characteristics of viscoelastic materials with varying structural properties expressed as a function, called viscoelastic functionally graded materials (VFGM).

VFGM are essentially isotropic or anisotropic viscoelastic materials where the properties are derived analytically and by manufacturing processes. Generally, the VFGM is spatial/temporal piecewise or entirely continuous functions with Cartesian coordinates x = {x1, x2, x3}. Real world examples are composites, two or more dissimilar homogeneous media, and polymers with distinct tension/compression moduli, etc. [2]

The design process starts by identifying the target performance, such as the isolation of vibration, minimization of the deflection amplitude, weight, or costs. The next step is to determine the material function to meet a specified design target, requiring the formulation of governing equations to express the mechanical behavior of the system. The design variables required to express the character of the material must then be identified.

During the process, one must take into account

- what is the best possible mathematical model that accurately represents the mechanical behavior of the system with solvable equations
- what are the limitations of the model, where some phenomenon are properly characterized and some are not all

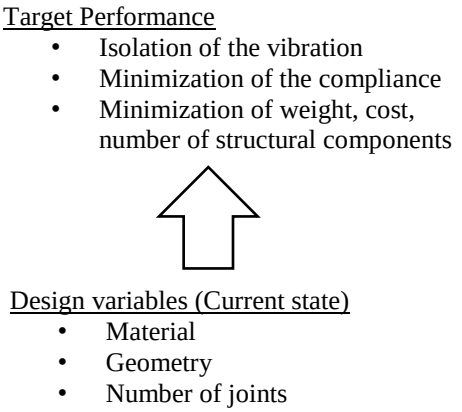

Figure 1.1 The inverse problem of structural design

In Figure 1.1, the flow of structural design in the current framework is depicted where an optimal material function is solved from the design variables expressing the current state to achieve the target performance.

Many previous publications have addressed the material distribution optimization of the *instantaneous elastic modulus* for linear viscoelastic problems with the *relaxation behavior* defined by the user by fitting Prony series to experimental data. While these projects have proven that significant improvements in the performance can be achieved compared to the optimal distribution problem of the elastic material, they fail to take advantage of varying the *relaxation behavior* of the viscoelastic material. Additionally, previous publications have oversimplified the dynamic behavior of the system by assuming the torque on the system is *independent* from the structural response, which does not apply to many dynamic and aeroelastic problems.

For this work, the following approach was taken:

1) The selection of the design variables for an optimization problem for linear viscoelastic materials requires attention compared to elastic materials (i.e. the Young's and shear moduli) to insure that the problem includes the most general material behavior. For the present work, the time dependent relaxation shear modulus G(t) was selected as the design variable.

2) In order to more accurately assess the result of the method when applied to actual dynamical systems, the problem was defined as a closed-loop system where there is feedback between the structural response and torque.

The motivation of this research is to outline a mathematical/computational framework for the material distribution optimization problem of a linear viscoelastic material. The distribution of the *relaxation behavior* (coefficients of the Prony series expansion) across the system was obtained to achieve a target performance of the dynamic system by the particle swarm optimization (PSO) method. To demonstrate the validity of the proposed method, an optimization problem was performed on a twisting shaft under a time dependent torque with distributed linear viscoelastic material properties.

1.1 Structural design optimization

The structural design problem in the current framework is an *inverse* problem where an optimal material distribution is solved for an objective function from the design variable(s) defining the current state. The working domain is defined as a physical region where the material will be distributed, represented by Δ. The material domain is given by Ω. The optimization problem is to determine the optimal material distribution Ω^* to minimize the cost function f_0 subscribed to design constraints *c*. The cost and constraint functions are dependent on the state variables, such as the displacement field *u*, which has direct dependence on the material distribution Ω.

Mathematically, the generalized optimization problem can be written as:

$$\begin{aligned} &\min_{\Omega \subset \Delta} f_0(\Omega) \\ &\text{Subject to : } \mathrm{c_i}(\Omega) \geq 0, i = 1,2,3,\ldots \\ &\qquad\qquad \widetilde{\mathrm{c}_\mathrm{j}}(\Omega) \geq 0, j = 1,2,3,\ldots \end{aligned} \tag{1.1}$$

Where $\mathrm{c_i}(\Omega)$ and $\widetilde{\mathrm{c}_\mathrm{j}}(\Omega)$ denote the equality and inequality constraints.

1.2 Related works

In the past, structural design optimization procedures were performed for linear elastic problems with material properties independent of time [3]. With the widespread use of compliant materials in recent years, the focus has shifted to nonlinear-elastic [4] and to viscoelastic materials [5]. Some publications on optimization focused on the modelling of the damping in the structure such as a two-phase composite [6] or laminated sandwich structure with a viscoelastic layer [7]. Many problems deal with topology optimization for a given viscoelastic material property and time independent loads [8~10]. Recent publications have expanded this problem to time

dependent loads [11,12]. Parameter identification of viscoelastic materials was done by global/local optimization solvers [13] or by fitting with experimental data [14].

For closed loop problems, there still does not exist much literature dealing with material distribution optimizations. Formulation of the 3D finite element modelling of the closed loop problem for active damping vibrating structures was done in [15]. The best control parameters to maximize the damping of the closed loop system was found in [16]. Both publications assumed either an uniform material distribution or a piezoelectric device on a patch of viscoelastic material. The optimization of viscoelastic supports for a rotating machinery using a hybrid optimization technique was done in [17].

1.3 Motivation

One advantage of distributing the relaxation behavior of the viscoelastic material is the control of the damping that is present in the material. In order to demonstrate the benefit of not only varying the instantaneous elastic modulus but also the damping, case studies were performed on the structural response of the system for simple distributions of the shear moduli and damping coefficients. The angular displacement at the free end was plotted. Two cases of applied torque were performed: the first is a at the end of the shaft, where the objective is to suppress the *vibration* from a given amplitude. The second is a at the root of the shaft for which the objective is to suppress the *maximum amplitude* at the free end.

1.3.1. Influence of the shear moduli to the structural response

Three cases of the shear moduli distribution studied are shown in Figure 1.2.

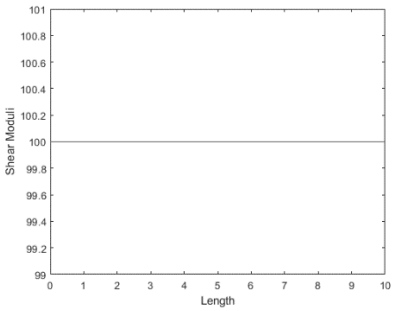

Case (a) Constant

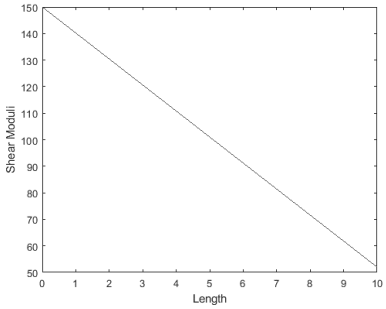

Case (b) Decreasing from root to tip

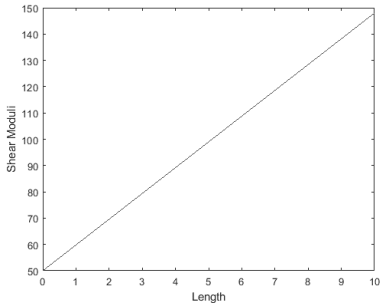

Case (c) Increasing from root to tip

Figure 1.2 Cases of shear moduli distributions

The first problem is a response to an initial condition with a torque at the end of the shaft, resulting in a sinusoidal angular displacement across the length. The root is fixed with no constraint at the free end. This indicates that the same boundary condition is applied for all coefficients other than the ones at the root. The problem is to suppress the angular displacement across the shaft at the minimum settling time. Figure 1.3 shows the plot of the angular displacement at the free-end with respect to time.

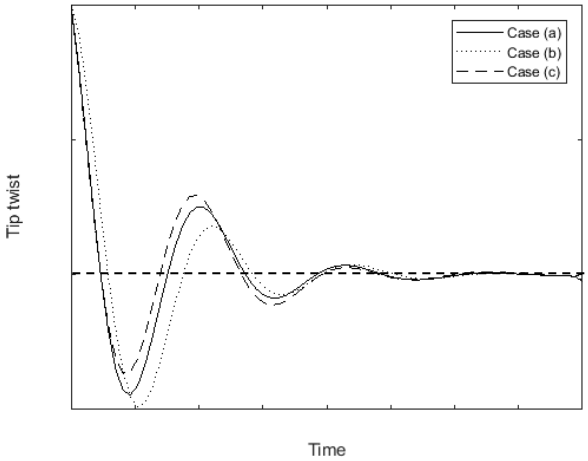

Figure 1.3 Comparison of angular displacement at the free-end with an initial torque at the free end

There is little differences in the amplitudes and settling times between the three cases. Initially, Case (c) with a *higher* modulus at the tip has a smaller amplitude compared to Case (b) with a *lower* modulus, but the later oscillations show slightly higher amplitudes. This is since the oscillation amplitude at the free-end is dependent on the entire shaft stiffness at the root of the shaft.

The second response examined is an initial condition with a torque at the root of the shaft. Again, the root is fixed with no constraint at the free end. The problem is to suppress the maximum angular displacement at the free end of the shaft. Figure 1.4 shows the plot of the angular displacement at the free-end with respect to time.

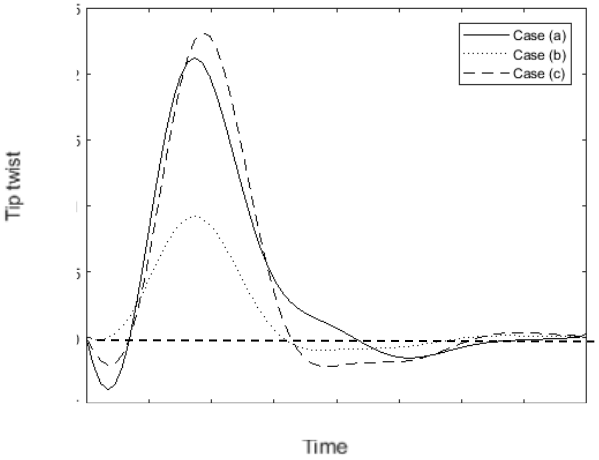

Figure 1.4 Comparison of angular displacement at the free-end with a instant torque at the root

Case (b) with *higher* moduli at the root shows a much smaller amplitude than the other two cases with *lower* moduli at the root. After the first oscillation all three cases show random oscillations until settling.

By effectively distributing the modulus, the maximum angular displacement can be reduced, but the settling time of the system cannot be controlled.

1.3.2 Influence of damping on the structural response

To study the influence of damping on the response of the structure, three simple cases of distribution of damping were studied with the shear moduli constant across the span. It is worth noting that the problem is still elastic, and the damping is the property of the shaft, not the material.

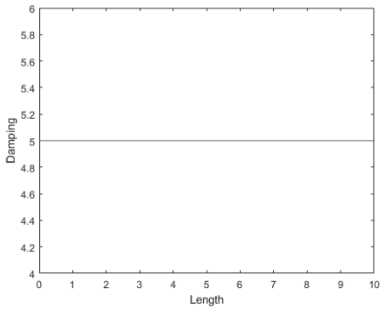

Case (e)
Constant damping across the length

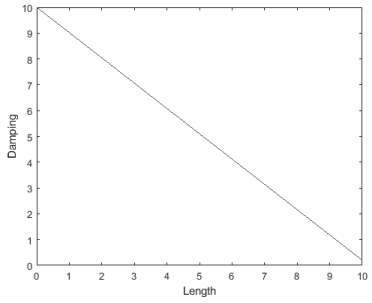

Case (f)
Decreasing damping from root to tip

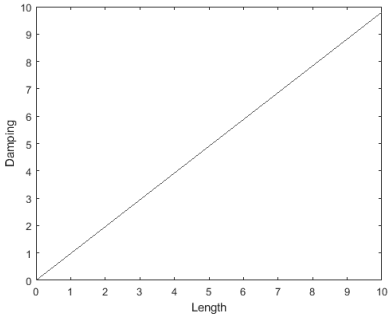

Case (g)
Increasing damping from root to tip

Figure 1.5 Cases of damping coefficient distribution

The response examined is an initial condition with a torque applied at the free end. The root is fixed with no constraint at the free end. The problem is to suppress the oscillation of the shaft free end subjected to an instantaneous torque. Figure 1.6 shows the plot of the angular displacement at the free-end with respect to time.

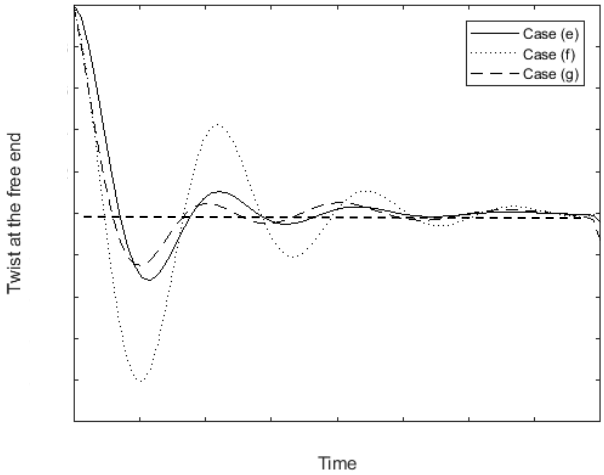

Figure 1.6 Comparison of angular displacement at the free-end with a initial torque at the free end

Case (f) with a *small* damping at the free end has a large oscillation amplitude compared to the other two cases since a high damping at the location of high oscillation will reduce the amplitude. It is worth noting that there is a small shift in the phase between the cases.

By varying the distributing of the damping coefficient, there is a noticeable change in the amplitude of the oscillation and settling time. Therefore, by strategically distributing not only the instantaneous moduli but also the relaxation behavior, a larger change in the dynamic behavior of the system can be expected.

1.4 Contributions of this thesis

By applying a material distribution optimization to a realistic closed loop system, the goal is to expand the use of structural optimization in designing real-life dynamic systems with compliant mechanics. The contributions of this thesis can be summarized as follows:

1. Conduct a compliant material distribution optimization problem for a *closed system,* where the torque change with respect to the output

2. Obtain the Prony series coefficients that express the viscoelastic material property by the PSO method (Previous papers have *prescribed* the relaxation behavior of the material)

1.5 Thesis outline

Chapter 2 formulates the mathematical model for the closed loop system that will be used for the discussion. The viscoelastic material properties is expressed as a Prony series expansion. The optimization methodology is discussed.

Chapter 3 demonstrates the validity of the proposed method by performing several examples with varying objective functions. The convergence capability of the method is shown.

Chapter 4 concludes the thesis.

CHAPTER 2
PROBLEM FORMULATION

This chapter builds the mathematical formulation of a structural design optimization problem to optimize the objective function expressing the performance of a system that depends on the relaxation behavior of the constructed material. This system for this paper is a shaft fixed at the root and free at the end with an applied torque. The dynamic system is under torsion at initial condition, causing an unwanted angular displacement in the structure. In a real-life system, such as a launch vehicle or aircraft wings, it would be ideal if the response can be eliminated entirely, or the time of oscillation be minimized to mitigate the damage to the equipment and/or errors of the onboard sensors which may otherwise lead to the failure of the mission.

2.1 Model of the viscoelastic material property

A widespread approach to linear viscoelastic analysis is to model the material as a generalized Maxwell and Kelvin models containing a combination of springs and dashpots arranged in series or parallel. Mathematically, the model can be represented as a Prony series function given as

$$G(y,t) = \sum_{j=1}^{N_p} G_j(y) e^{-\frac{t}{\tau_j}} \tag{2.1}$$

Where $G_1(y)$ with $\tau_1 = \infty$ is the instantaneous elastic shear modulus and N_p is the number of the Prony series terms. $G_j(y)$ are parameters that vary across the span that will be determined by the optimization procedure, while the values of the characteristic time scale τ_j will be subscribed. These values were subscribed not only to reduce the computational effort, but also since the relaxation behavior of the viscoelastic material can be expressed with subscribed values of the characteristic time scales equally spaced across the simulation time [11]. It is worth noting that when the characteristic time scales are prescribed, the values of the series lose their physical correspondence with the Maxwell and Kelvin models. Physically, the series describes the relaxation process, where at a constant applied strain the internal stress will gradually decrease in the material. For

characteristic deformation timescales longer than τ_j, the material transitions from the spring-like elastic behavior to dashpot-like viscous behavior.

The stress-strain relationship of the linear viscoelastic material can be expressed as

$$\sigma_{11}(\mathrm{y},\mathrm{t}) = \int_0^t \frac{E(t-t')\partial\varepsilon_{11}(y,t')}{\partial t'} dt' \tag{2.2}$$

By inserting Eq (2.1), the following expression is derived:

$$\sigma_{12}(\mathrm{y},\mathrm{t}) = \int_0^t 2E_j(y) e^{-\frac{t-t'}{\tau_j}} \frac{\partial\varepsilon_{12}(y,t')}{\partial t'} dt' \tag{2.3}$$

Dividing the time domain by N_t equal time steps, the discretized stress function becomes:

$$\sigma_{12}(\mathrm{y},\mathrm{t}) = \sum_{j=1}^{N_p}\sum_{i=1}^{N_t} e^{\frac{-t_{n+1}-t_i}{\tau_j}} \left(\frac{\tau_j}{\Delta t}\right)\left(1-e^{-\frac{\Delta t}{\tau_j}}\right) 2E_j(y) \ldots$$

$$[\sigma_{12,0}(y,t_i) - \sigma_{12,0}(y,t_{i-1})] \tag{2.4}$$

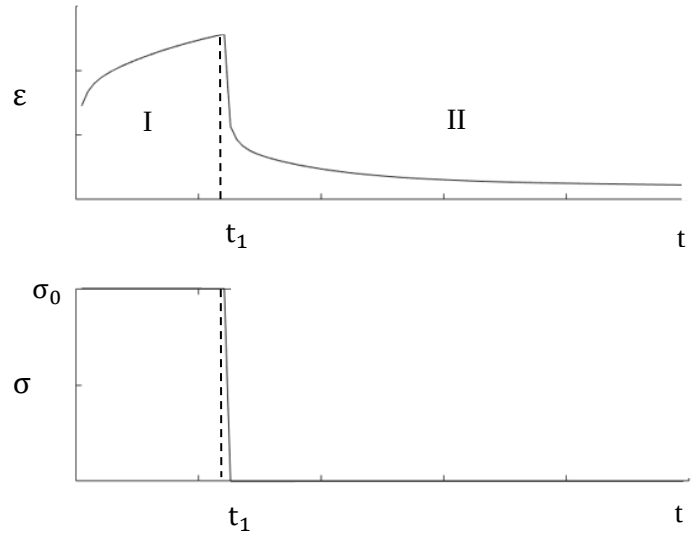

Figure 2.1 Creep curve of the viscoelastic material model

Figure 2.1 shows the torque (σ) and strain (ε) curves of a viscoelastic material under load. A constant torque ($\sigma = \sigma_0$) was applied until time t_1 at which the material was "instantaneously" unloaded. At constant torque in region I, the model shows the creep of the material which the rate of

change of the strain reduces with respect to time. At unloading in region II, the model captures the elastic after-effect of the material where the strain slowly trends towards zero.

2.2 Mechanical analysis

The system was modelled as a shaft fixed at the root and free at the end subjected to torsion, as shown in Figure 2.2. The relaxation moduli is distributed across the length of the shaft. The material property is assumed constant across the plane. The torque on the system is dependent on the angular displacement of the shaft, forming a closed loop system.

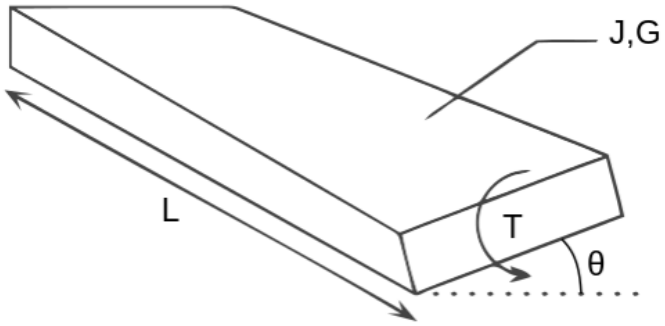

Figure 2.2 Twisting shaft problem

Mathematically, the dynamic closed-loop system is expressed as:

$$\rho\frac{\partial^2\theta(\mathrm{y,t})}{\partial \mathrm{t}^2}+\int_0^t\frac{\partial}{\partial y}\left(G(y,t-t')J_{eff}\frac{\partial^2\theta(y,t')}{\partial y\partial t'}\right)\mathrm{dt}'+\mathrm{K}\theta(y,t)=T \qquad (2.5)$$

ρ is the mass of the shaft, $\mathrm{J_{eff}}$ is the effective moment of inertia, T is an applied torque and K is a torsion parameter

With boundary conditions:

$$\theta(0,\mathrm{t})=0 \qquad (2.6)$$

$$\frac{\partial\theta}{\partial \mathrm{y}}(L,t)=0 \qquad (2.7)$$

At initial condition, a torque is applied on the shaft resulting in angular displacements across the length.

Performing the derivatives in equation (2.5),

$$\rho\frac{\partial^2\theta}{\partial t^2}+\int_0^t\left(\frac{dG(y,t-t')}{dy}J_{\text{eff}}\frac{\partial^2\theta(y,t')}{\partial t'\,\partial y}+\frac{G(y,t-t')J_{\text{eff}}\,\partial^3\theta(y,t')}{\partial t'\,\partial y^2}\right)dt'$$

$$+K\theta=T \tag{2.8}$$

Using the central difference method to discretize the equation with respect to time and space, the derivatives of the angular displacement can be expressed as the following:

$$\frac{\partial^2\theta(y,t')}{\partial t'\,\partial y}=\frac{(\theta_{i,k+1}-\theta_{i-1,k+1}+\theta_{i,k-1}-\theta_{i-1,k-1})}{2\Delta y\Delta t} \tag{2.9}$$

$$\frac{\partial^3\theta(y,t')}{\partial t'\,\partial y^2}=\frac{\theta_{i,k+1}-\theta_{i-1,k+1}-2(\theta_{i,k}-\theta_{i-1,k})+\theta_{i,k-1}-\theta_{i-1,k-1}}{\Delta t(\Delta y)^2} \tag{2.10}$$

where Δy and Δt express the length of increments in length and time, respectively. The subscript "i" is for stepping through time and subscript "k" for the length along the shaft.

The final discretized expression of the governing equation becomes:

$$\frac{\rho\left(\theta_{i+1,k}-2\theta_{i,k}+\theta_{i-1,k}\right)}{\Delta t^2}$$
$$+\sum_{j=1}^{N_p}\sum_{i=1}^{N_t}e^{\frac{-t_{n+1}-t_i}{\tau_j}}\left(\frac{\tau_j}{\Delta t}\right)\left(1-e^{-\frac{\Delta t}{\tau_j}}\right)\ldots$$
$$\left[\frac{G_{i,j+1}-G_{i,j-1}}{2\Delta y}J_{eff}\frac{((\theta_{i,k+1}-\theta_{i-1,k+1})+(\theta_{i,k-1}-\theta_{i-1,k-1})}{2\Delta y\Delta t}\right.$$
$$\left.+G_{i,j}\,J_{eff}\,\frac{\theta_{i,k+1}-\theta_{i-1,k+1}-2\left(\theta_{i,k}-\theta_{i-1,k}\right)+\theta_{i,k-1}-\theta_{i-1,k-1}}{\Delta t(\Delta y)^2}\right]\ldots$$

$$+K\theta_{i,j}=T_{i,k} \tag{2.11}$$

2.3 Optimization approach

The objective of the optimization problem is to find the optimal distribution of the relaxation behavior across the length of the shaft that maximizes/minimizes the objective function. The method chosen was the *constrained* particle swarm optimization (PSO) method due to its low cost when applied in nonlinear problems with numerous design parameters.

PSO is a stochastic global optimization method exploiting a set of potential solutions to search the solution space. It relies on the exchange of information between potential solutions. Each "particle" adjusts its trajectory towards its own previous best position and the best previous position attained by any member of its neighborhood. Global sharing of information enables particles to utilize discoveries and previous experience of others during the search for promising regions of the problem space.

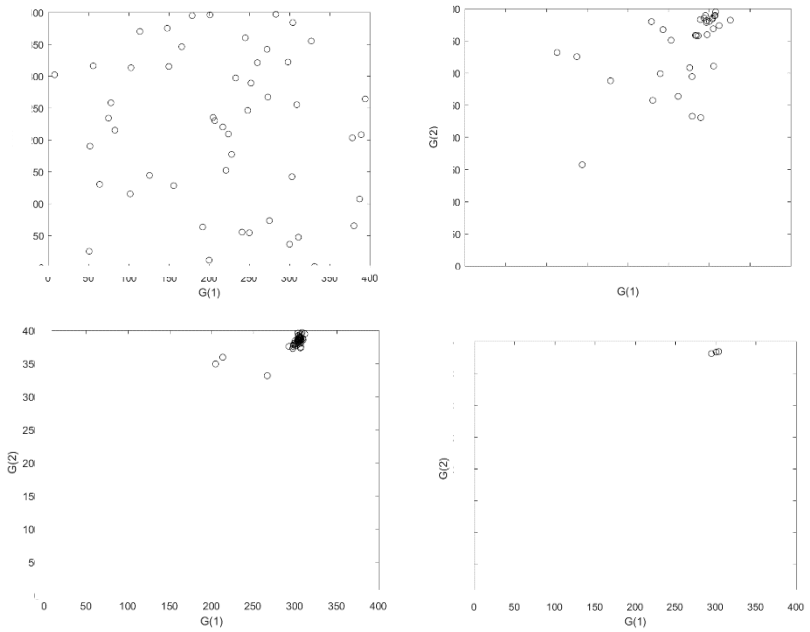

Figure 2.3 Evolution of the solutions for a two parameter problem

Figure 2.3 shows the evolution of the potential solutions when the PSO method is applied to a two-parameter problem. The figure on the top-left shows the initial randomly distributed solutions. The top-right shows the potential solutions after several iterations where they are distributed in a more concentrated region in the solution space. The bottom two figures show the process of the particles converging to a single, optimal solution.

The optimization procedure can be summarized as the following [18]:

1. Initialize the design variables for each of the N particles

a) Initialize the design parameters $G_i(0)$
b) Initialize the best position of the particle to its initial position $p_i(0) = G_i(0)$
c) Calculate the current global best g_i of the particles at the initial position

2. Repeat the steps until the stopping criteria is met

a) Update the particle velocity according to equation (2.11)
b) Update the particle position according to equation (2.12)
c) Update the personal best p_i if $f\big(G_i(t+1)\big) < f(p_i)$
d) Update the global best g_i if $f\big(G_i(t+1)\big) < f(g_i)$
e) Reduce the inertia mass parameter w for each iteration

The expressions for updating the solutions are given as:

$$\mathrm{V_n^{m+1}} = wV_n^m + z_1 r_1 (p_n^m - G_n^m) + z_2 r_2 (g_n^m - G_n^m) \qquad (2.12)$$

$$G_n^{m+1} = G_n^m + V_n^{m+1} \qquad (2.13)$$

where n = 1, 2, …N, and N is the size of the population of the particles, w is the inertia mass, m is the iteration number, p is the particle's local best, and g is the global best of the entire "swarm". z_1 and z_2 are constants called the cognitive and social parameter respectively, r_1 and r_2 are random numbers uniformly distributed within the range [0 1].

In order to enforce the constraints on the Prony series coefficients ($\mathrm{G_i}$) values as the solutions of the particles are updated based on the local and global optimal solutions for every iteration, a penalty function was included in the objective function.

The objective function was rewritten as,

$$\min_{G_i \subset \Delta} f_0(G_i) + P(G_i) \qquad (2.14)$$

Subject to: $\mathrm{c_i}(G_i) > 0$

Where P is the penalty function defined as:

$$\mathrm{P}(G_i) = \begin{cases} 0 & G_i \in R^n \\ \sum_{i=1}^{m} c_i (G_i)^2 Q_i & G_i \notin R^n \end{cases} \tag{2.15}$$

Q_i is the penalty factor which depends on the degree of violation. It is worth noting that the penalty function is non-zero only when the constraints are violated.

In addition to the penalty function, a potential solution that violated the constraint at an extreme degree in order to obtain the optimal value was "reset" to a random point within the solution space. This was added since several particles would overcome the penalty function, resulting in fewer viable potential solutions in the solution space and a misleading information to other potential solutions. This was preferred over changing the values of the penalty factor Q_i for each problem, which would increase the time to setup each problem.

It is worth noting that the PSO method has many constants that must be adjusted by the user for every problem, including the cognitive and social parameters z_1 and z_2 which defines the step sizes the "particles" take for every iteration and the penalty factor Q_i which adjusts the penalty applied to the objective factor to guarantee the constraints are satisfied. While this is a large drawback of the method, the PSO method was shown to be more computationally efficient and consistent compared to the conventional Monte Carlo algorithm. [19] Additionally, the recent advancements in the method, including a publication proposing to add the Monte Carlo algorithm to the PSO to further increase the computational efficiency [20], has further enhanced the viability of the method. While exploring the best computational algorithm for the given problem was beyond the scope of this project, it would be meaningful for future works to determine an algorithm to efficiently optimize complex systems with numerous design variables.

2.4 Convergence analysis of the algorithm

The rate of convergence of the algorithm ensures that an optimum can be reached within an appropriate computational time. In order to illustrate the convergence capability of the proposed method, the different types of fitness functions were calculated for each case. Table 2.1 shows the definition of the types of fitness functions.

Table 2.1 Types of fitness functions

	Definition
Average fitness (F_A)	Average fitness of all particles in an iteration
Mean fitness of the best particle (F_{BPA})	Average fitness of the best positions of each particle
Mean fitness of the global best particle (F_{GBA})	Average fitness of the best global positions of each iteration
Global optimal fitness (F_{GB})	Best global fitness up until the iteration

The fitness of the fitness (F) can be found from the equation [21]:

$$F_j = \frac{1}{N_r N_{pop}} \sum_{k=1}^{N_r} \sum_{i=1}^{N_{pop}} f_{ij}(X) \tag{2.16}$$

where N_r is the number of iteration, N_{pop} is the number of the swarm population, f is the objective function, and X is the parameter being optimized. For calculating the mean fitness of the best particle (F_{BPA}), X is replaced by X_i^b, the best position found by the particle. When calculating global optimal fitness (F_{GBA}), X is substituted by X_g^b, the global best position of the particle, and N_{pop} is set as 1.

CHAPTER 3
RESULTS AND DISCUSSION

In order to demonstrate the validity of the proposed method, an optimization was performed for different objective functions. The parameters determined were the Prony series coefficients (G_i) that express the distribution of the linear viscoelastic relaxation behavior across the shaft. Five Prony series coefficients (G_i) were used to express the relaxation behavior at each node across the length of the shaft with prescribed characteristic time scales. With 20 nodes distributed equally across the shaft length, the problem was to determine the values of 100 Prony series coefficients to optimize a given objective function. After the method was performed, the displacement field after the optimization was compared with the displacement field before the optimization to show the change in the structural response. The convergence capability for each simulation case is discussed.

Table 3.1 summarizes the objective functions and torque applied on the shaft for three simulation cases.

Table 3.1 Objective function and torque of the optimization cases

Section	Objective function	Torque
3.1.1	Minimize the angular displacement after torsion	Constant until $t_{end}/4$, acting on the free end
3.1.2	Minimize the angular displacement across the entire time span	Constant until $t_{end}/4$, acting on the free end
3.1.3	Best fit between the target and simulated free end angular displacements	Acting on the free end and gradually decreasing with respect to space and time

The first simulation is a constant torque at the free end until $t_{end}/4$, causing an unwanted angular displacement across the shaft. To demonstrate that the method can be applied to suppress specific structural responses, the objective function was set to minimize the angular displacement across the shaft *after torsion*.

The second simulation is the same torque as the first. The difference is the objective function which is set to minimize the angular displacement across the shaft for the entire time span. Here, more nodes of the displacement field must be adjusted in order to achieve a global optimum. The difference in the convergence capability between the first and second simulation will be discussed.

The third simulation is to determine a distribution of the relaxation behavior that will achieve a target free end angular displacement for a given torque. The torque was set to be a continuous function to compare the results the previous cases with instantaneous loading and unloading.

The constraints applied to the problem were identical for all cases:

- Boundary conditions (2.6) and (2.7)
- $0 < G(i) < 200$
- Number of Iterations < 50

The number of iterations was set after adjusting the PSO constants and determining the minimum that's required to reach a optimum. The constraint on the Prony series is set above 0 since a negative value has no physical meaning. The maximum value is set such that the series values does not go to infinity during the optimization procedure.

Table 3.2 summarizes the values of the PSO constants for all three cases. The *cognitive coefficient* was set smaller than the *social coefficient* to prompt convergence within the given number of iterations. While this means that a smaller solution space is explored, given the large number of coefficients, it was unrealistic to thoroughly explore every solution within the solution space in a reasonable computational time. In order to assure the reliability of the result, the same simulation was performed several times with different initial distributions of potential solutions. The *inertia mass* was reduced as the simulation reaches later iterations since it is preferred for the particles to have large step sizes at early iterations to explore the solution space before "slowing down" to converge to a single solution.

Table 3.2 Value of the constants of the PSO method

	Value	Definition
Cognitive coefficient (z1)	0.1	Weight of the local best location on the size of the step
Social coefficient (z2)	1.5	Weight of the global best location on the size of the step
Inertia mass (w)	• Initially 0.5, subtract 0.01 for each iteration	Degree of influence of the previous step size to the current step size
Number of particles	50	
Penalty factor (Q)	• "1" for violation of G(i) up to 100 • "10" for violation of G(i) up to 150 • "100" for violation of G(i) above 200	Ensures the solutions stay in 0<G(i)<200

3.1 Optimization results

3.1.1 Displacement suppression after torsion

For this case, given a constant torsion at the free end until $t_{end}/4$, the objective was to minimize the angular displacement after the torsion is diminished at $t_{end}/4$. The goal is to demonstrate that the method can be applied to design systems that can quickly suppress the effect of sudden unexpected torsion. Figure 3.1 shows the torque curve at the free end.

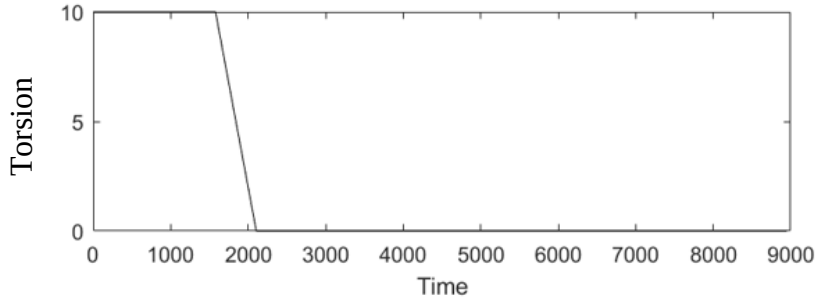

Figure 3.1 Torque applied on the free end with respect to time

Figure 3.2 shows the angular displacement at the free end on the initial and final iterations. The optimized solution suppresses the increasing displacement after $t_{end}/4$ in the initial iteration effectively. There is also a decrease in the maximum angular displacement during torsion which is

caused the adjustment of the relaxation behavior at the free end to suppress the displacement after torsion.

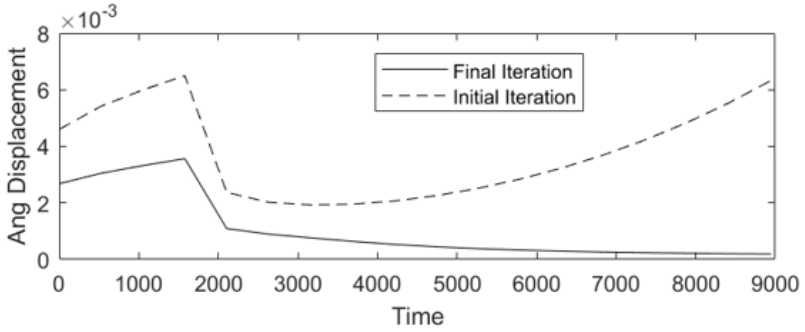

Figure 3.2 Angular displacement at the free end at initial and final iterations

Figure 3.3 shows the change in the value of the objective function across the iteration. From the first iteration, with randomly generated Prony series coefficient values, there is more than 50% improvement as the function settles close to the 20th iteration. The convergence to a single value suggests that the simulation has reached an optimum. The function is degrees smaller than the displacements since it is a square of the angular displacement field.

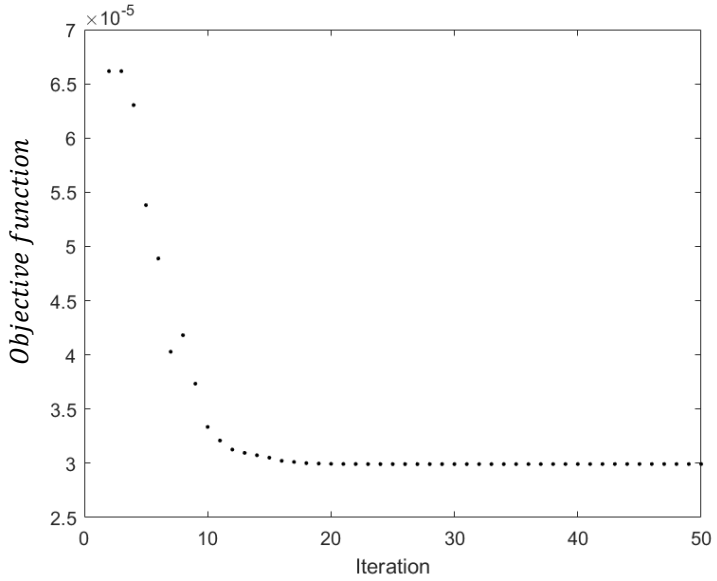

Figure 3.3 Change in the global best of the fitness function after $t_{end}/4$ for every iteration

Figure 3.4 shows the angular displacement across the length and time after the optimization. The displacement field shows that the optimal solution effectively suppresses the displacements after twisting across the length of the shaft.

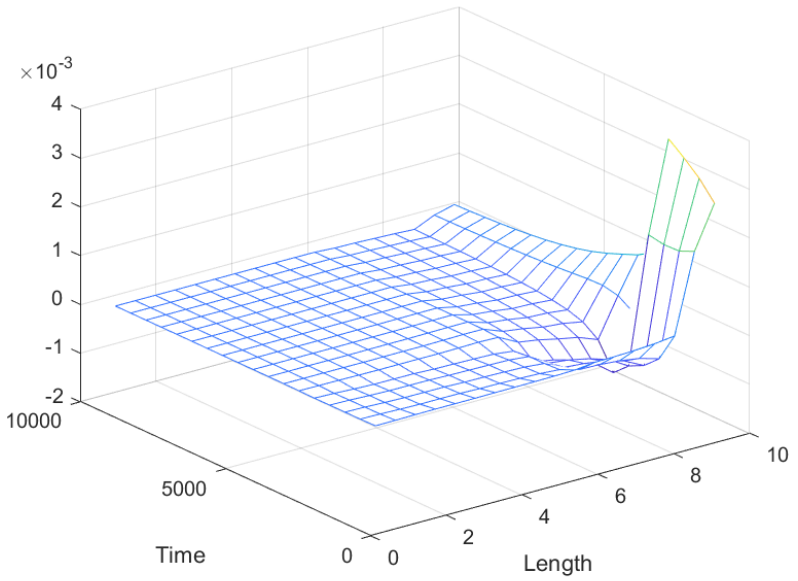

Figure 3.4 Optimized angular displacement across length and time

Figure 3.5 shows the optimally distributed relaxation behavior across the length of the shaft. There is a large discrepancy of the initial value of the modulus across the length of the shaft. One reason may be the computational instability caused by the by the instantaneous application and removable of the torque.

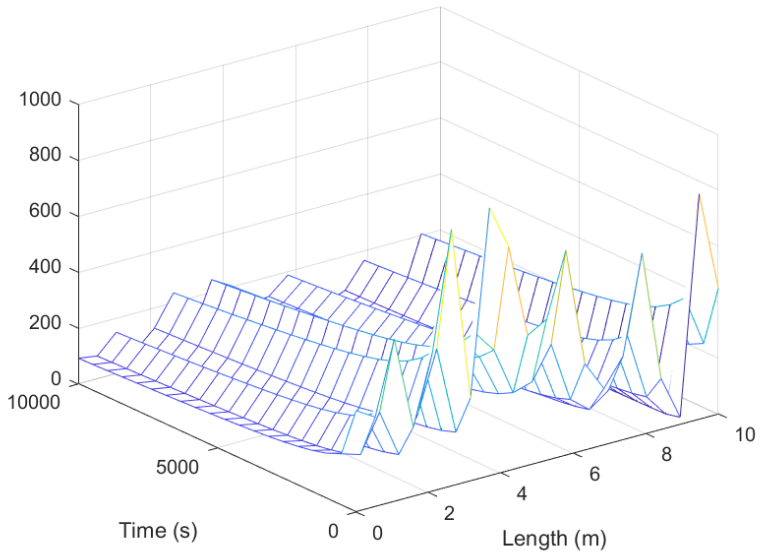

Figure 3.5 Optimized distribution of the relaxation behavior across the length

3.1.2 Minimum displacement across the entire time span

For this case, the objective was to reduce the displacement across the entire time span. The shaft was under constant torque at the free end until $t_{end}/4$. Figure 3.6 shows the angular displacement fields of the initial and final iterations. It can be seen that the method effectively suppresses the displacement across the length of the shaft during torsion. The maximum angular displacement at the free end is also reduced.

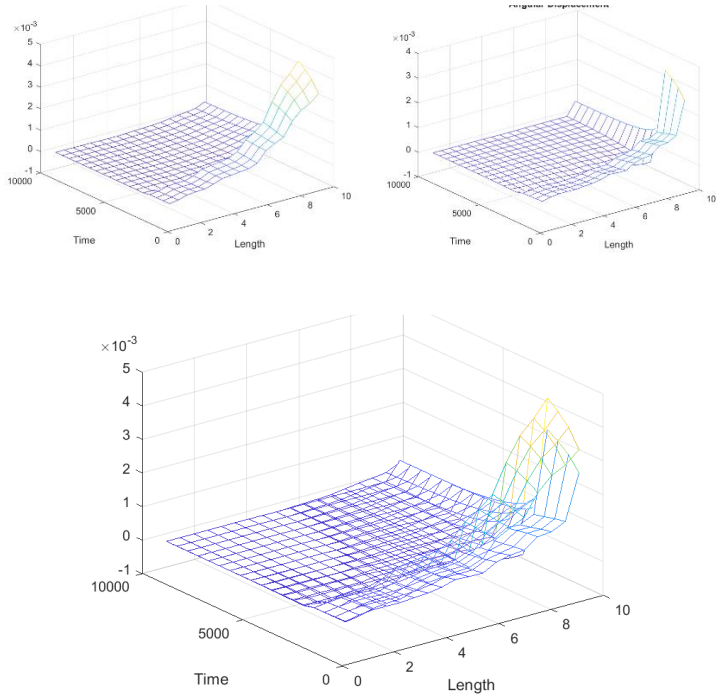

Figure 3.6 Angular displacement field at initial iteration (top left), final iteration (top right), and the two surfaces in the same figure (bottom)

Figure 3.7 shows the decrease in the objective function as the method searches for the global minimum. The simulation settles at a minimum value at around the 20th iteration. There is about a 35% decrease in the angular displacement from the initial to final iteration.

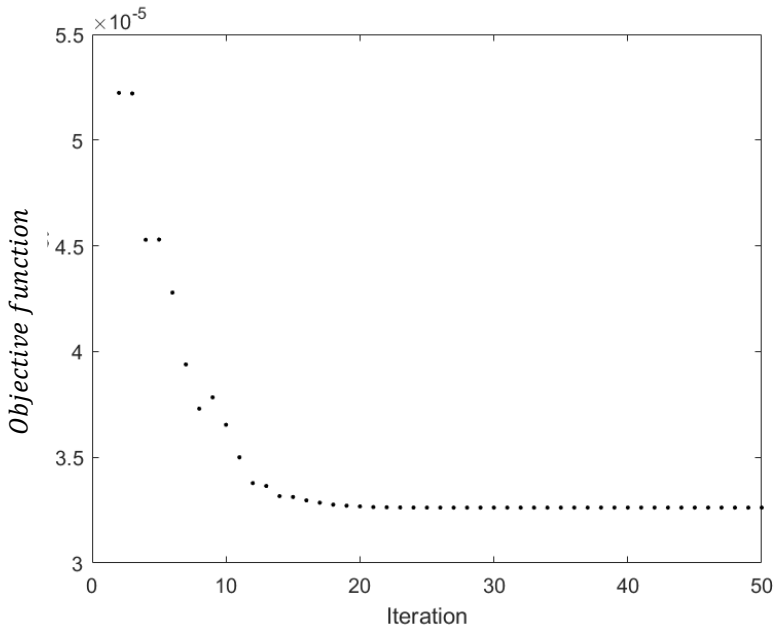

Figure 3.7 Change in the global best of the angular displacement squared for every iteration

Figure 3.8 shows the optimized relaxation behavior distribution across the length of the shaft. As in the previous case, there is large discrepancy of the moduli across the length of the shaft at initial time.

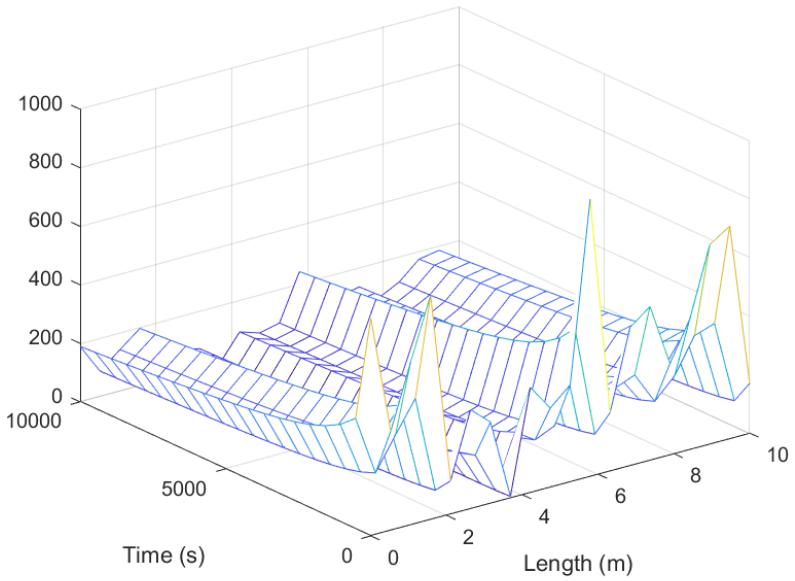

Figure 3.8 Optimized distribution of the relaxation across the length of the shaft

3.1.3 Fitting the free end displacement to a target value

For the final case, a continuous torque was applied at the end of the shaft, as shown below in Figure 3.9. Unlike the instantaneous unloading in the previous two cases, the torque gradually decreases in both time and space, forming a pyramid-like function. The objective function was to set the angular displacement at the free-end to a target value. Again, this is different from the previous cases where the objective was to minimize the structural response.

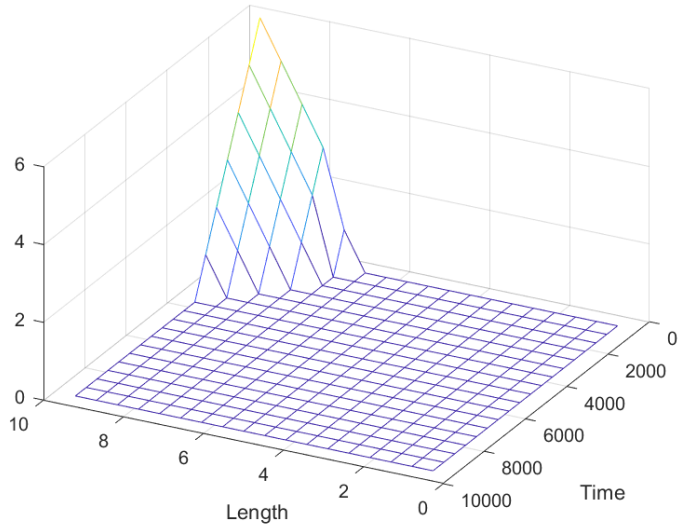

Figure 3.9 Torque distribution for simulation 3.1.3

Figure 3.10 below shows the free end angular displacement and torque plotted with respect to time for two cases. Case (a) is similar to the previous simulations, where the objective function was set to eliminate the angular displacement at the free end. For Case (b), the goal was set to the free end angular displacement at 2e-3. Case (b) converges to the target angular displacement faster than Case (a) due to the smaller difference between the maximum displacement during loading and target displacement.

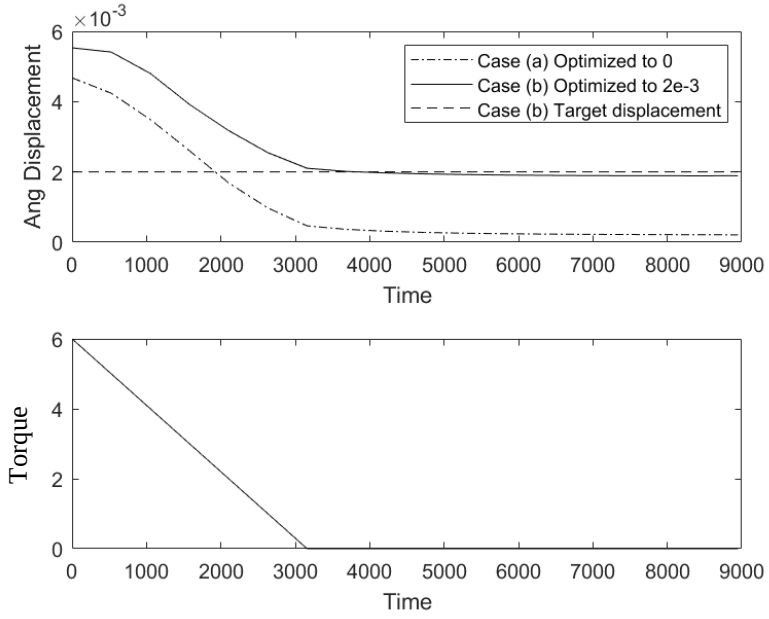

Figure 3.10 Angular displacement and torque at the free end

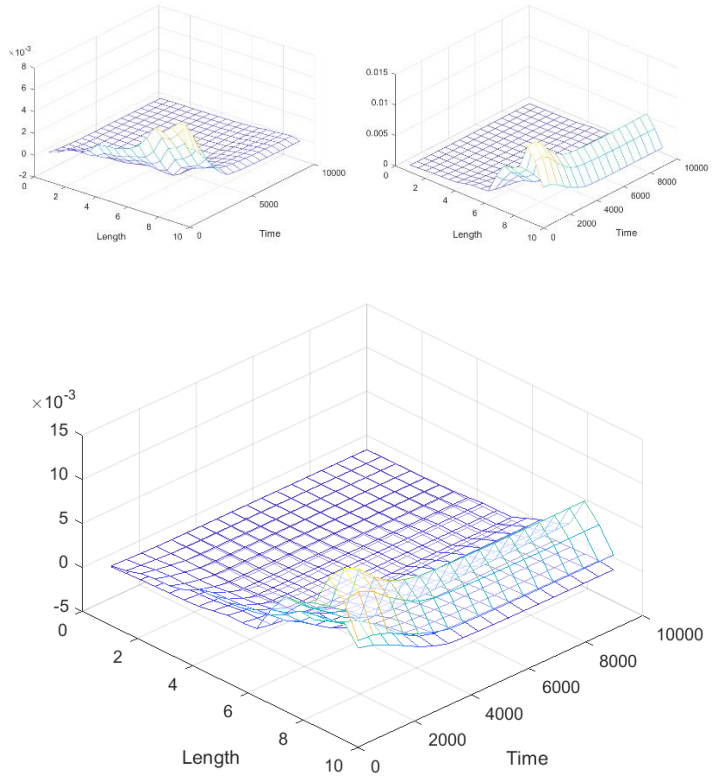

Figure 3.11 Angular displacement of Case (a) [top left], Case (b) [top right] and both surfaces in the same figure [bottom]

Figure 3.12 shows the optimal distribution of the relaxation for both cases. The main difference between the two are the initial shear moduli values near the free end. Case (a) shows an increase in the moduli from the free end whereas Case (b) shows a gradual decrease from the free end. As a result the maximum angular displacement for Case (b) occurs away from the free end and twisting the free end to the target displacement. It is worth noting that the discontinuity across the length still persists with continuous torque applied on the system.

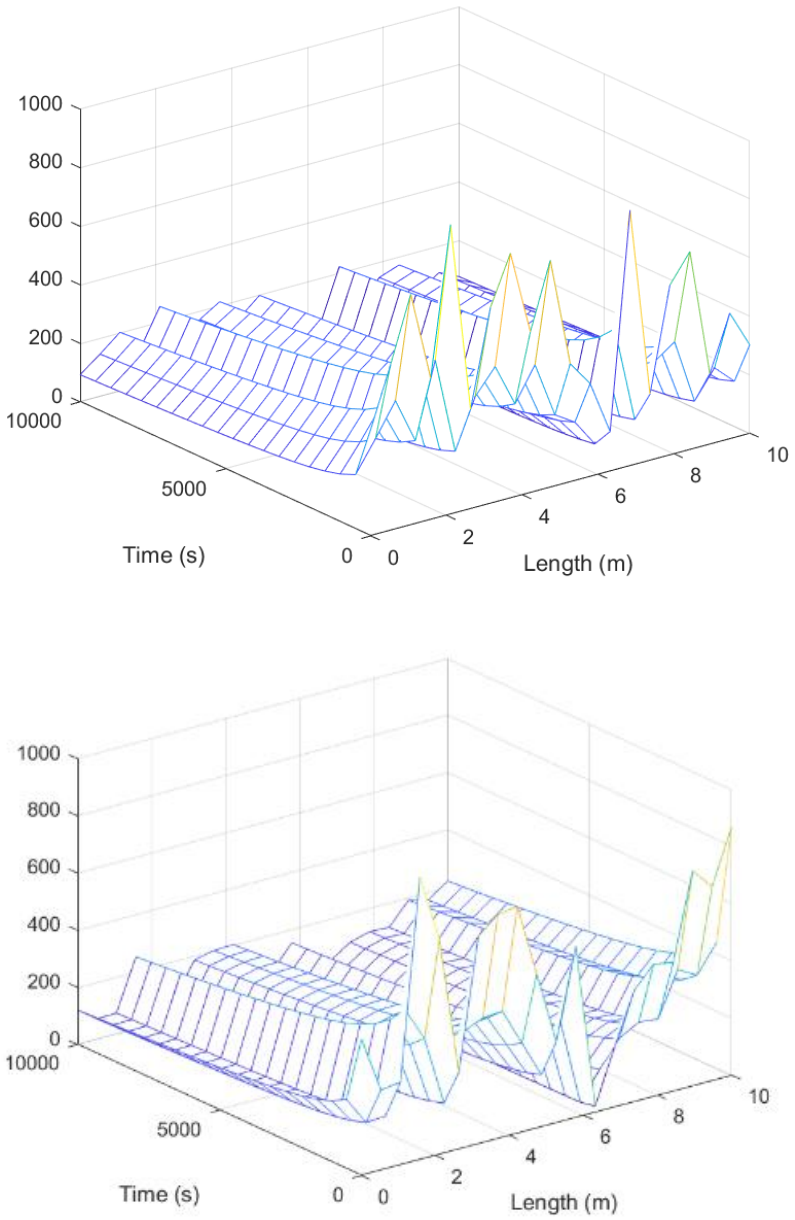

Figure 3.12 Optimized distribution of the relaxation across the length of the shaft for Case (a) [top] and Case (b) [bottom]

3.2 Convergence capability

To ensure that the proposed algorithm is able to converge to a solution in an acceptable computational time, the convergence capability of the method was explored. Varying types of fitness functions were plotted for each simulation cases to determine the convergence for varying objective functions.

Figure 3.13 shows the plot of the various fitness functions defined in the previous chapter with respect to the iteration. Both the *global best* and the *best particle average* fitness functions reach the same values at around the 30th iteration. This indicates a high reliability of the results since all the particles have reached a single solution from both local and global position sharing. It is worth noting that the *best particle average* fitness function is plotted from the 5th iteration onwards. This is due to the high fitness values by some particles violating the constraints while exploring the solution space.

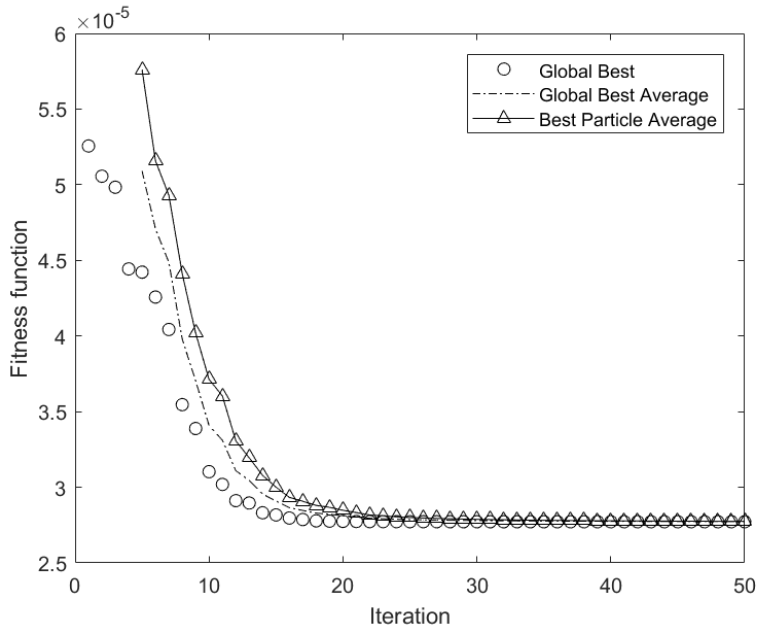

Figure 3.13 Comparison of fitness across the iterations for simulation (3.1.1)

Figure 3.14 shows the *average fitness* of all the particles across the iterations of the method. Unlike Figure 3.13 above which plots the information stored to be used in the optimization procedure, the figure plots the actual "movement" of the particles. It is plotted from the 5th iteration due to some particles violating the constraints at the early iterations. Since the function converges at a fast rate, the convergence capability is high, but with less exploration of the solution space.

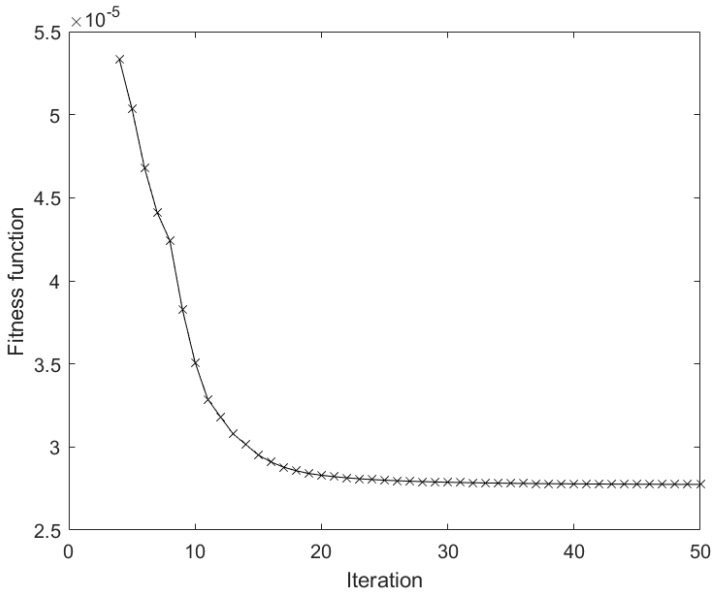

Figure 3.14 Average fitness of particles for simulation (3.1.1)

Figure 3.15 shows the various fitness functions for simulation (3.1.2). It can be noted that the *best particle average* and the *global best* do not converge which indicates there were some particles that got "stuck" in a local minimum. This indicates that the solution space explored during the computation may not be the most optimal due to local sharing of particle position. This can be avoided by increasing the *inertia mass* which allows the particles to search the solution space thoroughly.

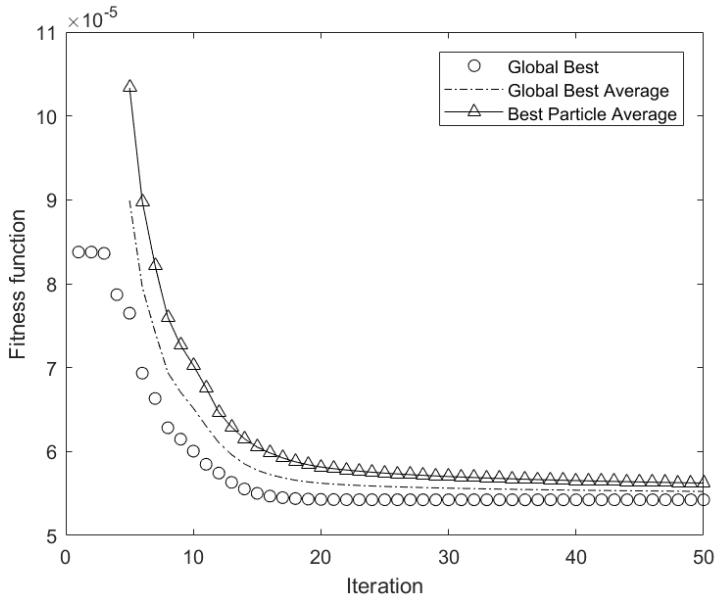

Figure 3.15 Comparison of the fitness function for simulation (3.1.2)

Figure 3.16 shows the average fitness of the particles for the simulation. The convergence is slower compared to that of simulation (3.1.1), which may be caused by the larger number of displacement nodes values that was adjusted for the optimization. The particles still converge at within an acceptable computational time.

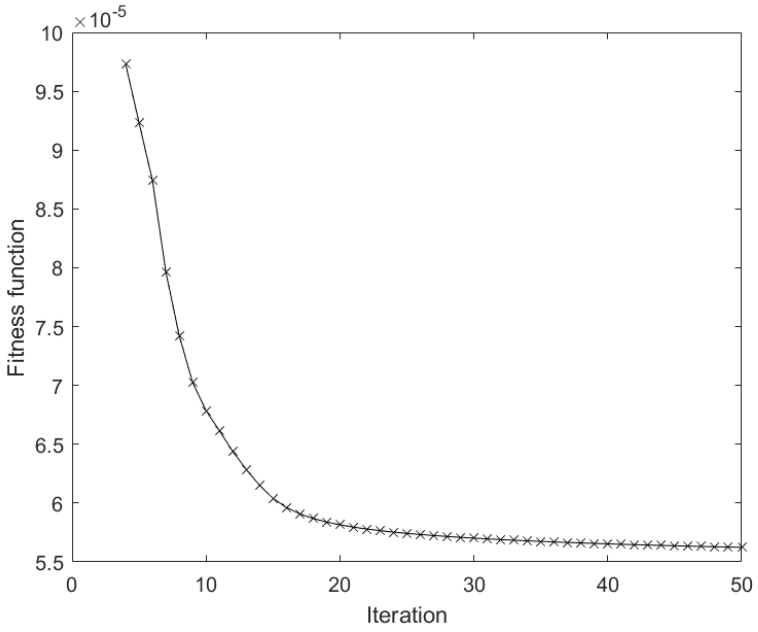

Figure 3.16 Average fitness of particles for simulation (3.1.2)

Figure 3.17 shows the fitness function for the final simulation where the free end displacement was set to a target value. Like that of simulation (3.1.1), both the *best particle average* and the *global best* converge to a single value indicating reliable results. The value of the fitness function is a degree smaller than the previous cases since the maximum torque applied was less.

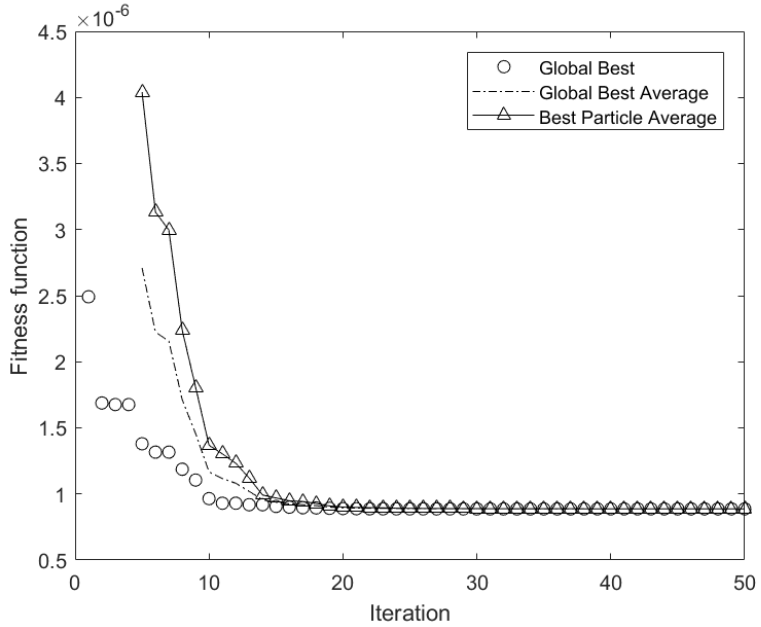

Figure 3.17 Comparison of the fitness function for simulation (3.1.3) Case (b)

Figure 3.18 shows the average fitness of the particles for the final simulation. The convergence is fast compared to the previous cases. This result is consistent with the previous cases where the convergence rate is faster for problems with less nodes to be optimized. Changing the torque on the system does not have any influence to the convergence.

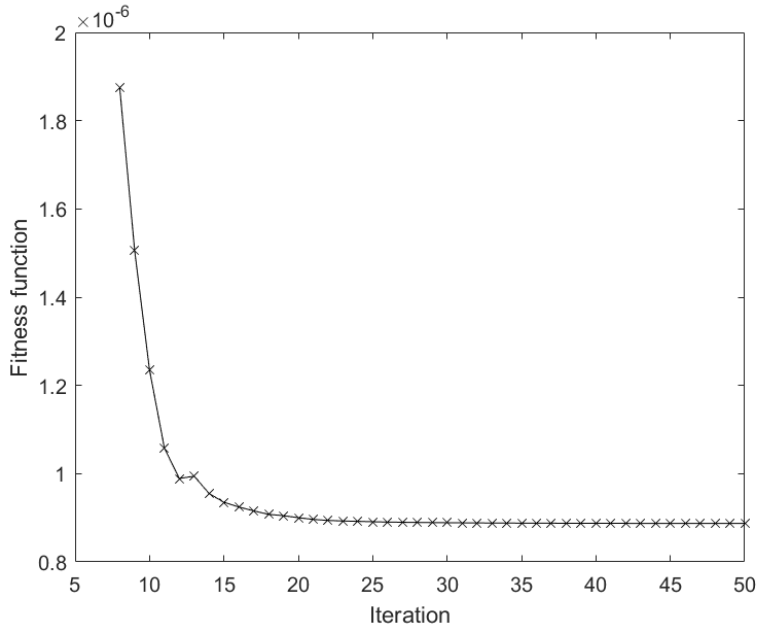

Figure 3.18 Average fitness of particles for simulation (3.1.3) Case (b)

CHAPTER 4
CONCLUSION

With rise of new manufacturing techniques, there has been an increase in attention in designing components with distributed material properties. Utilizing the benefits of compliant mechanics, a strategic distribution of the relaxation behavior of linear elastic materials was proposed. The particle swarm optimization (PSO) method was chosen due to its consistency in results and reasonable computation effort for non-linear problems. The proposed method was applied to a simple fixed shaft to demonstrate the improvement in the structural response of the system and convergence capability of the method. The simulations showed great improvement in the structural responses. The convergence capability analysis demonstrated that the method gives reliable results in an acceptable computational times. Additionally, the convergence time increased with the increase of the number of nodes that were optimized.

However, some problems of the method were:

- Inability to determine confidently the reaching of global minimum
- Lack of thorough search of the solution space to keep the computation time within a reasonable timeframe
- Discontinuity of the relaxation behavior across the length of the shaft is unrealistic for the actual manufacturing

The optimization of the relaxation behavior distribution requires adjustment of many parameters. In order to confidently reach the global minimum within a reasonable timeframe, the computational efficiency of the PSO method must be improved such that the particles can thoroughly search the entire solution space. Additionally, the exploration of the inclusion of additional constraints to ensure the a degree of continuity of the moduli across neighboring nodes must be done for the actual construction of the design.

REFERENCES

[1] Day, Dwayne A., "Composites and Advanced Materials" *U.S. Centennial of Flight Commission*. , 2003.

[2] Hilton, Harry H., Daniel H. Lee and Abdul Rahman A. El Fouly "General analysis of viscoelastic designer functionally graded auxetic materials engineered/tailored for specific task performances," *Mechanics of Time-Dependent Materials*, 12:151–178., 2008

[3] Rodrigues, H. C. and Fernandes, P. A. "Topology Optimization of Linear Elastic Structures Subjected to Thermal Loads," *Topology Design of Structures*, pp 437-450, 1993

[4] Bruns, T. and Tortelli, D. "Topology optimization of non-linear elastic structures and compliant mechanisms," *Computer Methods in Applied Mechanics and Engineering*, Volume 190, Issues 26–27, Pages 3443-3459, 2001

[5] Chen, W. and Liu, S., "Topology optimization of microstructures of viscoelastic damping materials for a prescribed shear modulus," *Structural and Multidisciplinary Optimization*, Volume 50, Issue 2, pp 287–296, 2014

[6] Prasad, J. and Diaz, A. R. "Viscoelastic material design with negative stiffness components using topology optimization," *Structural and Multidisciplinary Optimization*, Volume 38, Issue 6, pp 583–597, 2009

[7] Araújo, A. L., Martins, P., Mota Soares, C.M., Mota Sores, C.A., Herskovits, J. "Damping Optimization of Viscoelastic Laminated Sandwich Composite Structures," *Structural and Multidisciplinary Optimization*, 39:569, 2009

[8] El-Sabbagh, A. and Baz, A. "Topology optimization of unconstrained damping treatments for plates," *Engineering optimization*, Pages 1153-1168, 2013

[9] Behrou, R. and Guest, K. “Topology optimization for transient response of structures subjected to dynamic loads,” *18th AIAA/ISSMO Multidisciplinary Analysis and Optimization Conference AIAA AVIATION Forum*, AIAA 2017-3657, 2017

[10] Gao, T. and Zhang, W. “Topology optimization of multiphase-material structures under design-dependent pressure loads,” *International Journal for Simulation and Multidisciplinary Design Optimization*, Pages 297-306, 2008

[11] James, K. and Waisman, H. “Topology optimization of viscoelastic structures using a time-dependent adjoint method,” *Computer Methods in Applied Mechanics and Engineering*, Volume 285, Pages 166-187, 2015

[12] Yun, K. and Youn, S. “Multi-material topology optimization of viscoelastically damped structures under time-dependent loading,” *Finite Elements in Analysis and Design*, Volume 123, Pages 9-18, 2017

[13] Fernanda, *M.,* Costa, *P.* and Ribeiro, C. “Parameter Estimation of Viscoelastic Materials: A Test Case with Different Optimization Strategies,” *AIP Conference Proceedings*, Volume 1389, Issue 1, 2011

[14] Liu, K., VanLandigham, Mark R., and Ovaert, T. “Mechanical characterization of soft viscoelastic gels via indentation and optimization-rootd inverse finite element analysis,” *Journal of the Mechanical Behavior of Biomedical Materials*, Volume 2, Issue 4, Pages 355-363, 2009

[15] Lim, Y., Varadan, V. and Lim, Y. “Closed loop finite-element modeling of active constrained layer damping in the time domain analysis,” *Smart Materials and Structures*, Volume 11, Number 1, 2002

[16] Wang, L. and Liu, Y. “Damping Optimization by integrating enhanced active constrained layer and active-passive hybrid constrained layer treatments,” *Journal of Sound and Vibration*, Volume 255, Issue 4, Pages 763-775, 2002

[17] Riberio, E., Perira, J. and Bavastri C. “Passive vibration control in rotor dynamics: Optimization of composed support using viscoelastic materials,” *Journal of Sound and Vibration*, Volume 351, Pages 43-56, 2015

[18] Parsopoulos, K. and Vrahatis, M. “Particle Swarm Optimization Method for Constrained Optimization Problem,” *Intelligent Technologies-Theory and Applications: New Trends in Intelligent Technologies*, 10.1109/ICSENS.2016.7808412 , IOS Press, 2002

[19] Homaifar, A., Qi, C. and Lai, S. “Constrained Optimization Via Genetic Algorithms,” *Simulation*, Volume 62, Issue 4, Pages 242-253, 1994

[20] Cavalcanti, L. and Fontana, E. “Monte Carlo and particle swarm methods applied to the design of surface plasmon resonance sensors,” *2016 IEEE Sensors*, 2016

[21] Gong, Hong-Fei, Chen, Zhong-Sheng and Zhu, Qun-Xiong and He, Yan-Lin. "A Monte Carlo and PSO based virtual sample generation method for enhancing the energy prediction and energy optimization on small data problem: An empirical study of petrochemical industries," *Applied Energy*, Elsevier, vol. 197(C), Pages 405-415, 2017

[22] Xia-Ting, Feng, Chen, B., Yang, C., Zou, H. and Ding X. “Identification of visco-elastic models for rocks using genetic programming coupled with the modified particle swarm optimization algorithm,” *International Journal of Rock Mechanics & Mining Sciences*, Volume 43, Issue 5, Pages 789-801, Elsevier, 2005